Chinese Chemical Letters 34 (2023) 107843

Contents lists available at ScienceDirect

Chinese Chemical Letters

journal homepage: www.elsevier.com/locate/cclet

In-situ assembly of 2D/3D porous nickel cobalt sulfide solid solution as superior pre-catalysts to boost multi-functional electrocatalytic oxidation

Pin Hao[a,1,*], Xu Dong[a,1], Houguang Wen[a], Ruirui Xu[a], Junfeng Xie[a], Qian Wang[a], Guanwei Cui[a], Jian Tian[b,*], Bo Tang[a]

[a] College of Chemistry, Chemical Engineering and Materials Science, Collaborative Innovation Center of Functionalized Probes for Chemical Imaging in Universities of Shandong, Key Laboratory of Molecular and Nano Probes, Ministry of Education, Shandong Provincial Key Laboratory of Clean Production of Fine Chemicals, Shandong Normal University, Ji'nan 250014, China
[b] School of Materials Science and Engineering, Shandong University of Science and Technology, Qingdao 266590, China

ARTICLE INFO

Article history:
Received 14 June 2022
Revised 4 September 2022
Accepted 21 September 2022
Available online 24 September 2022

Keywords:
Electrocatalytic oxidation
(Ni, Co)S_2 solid solution
Pre-catalyst
Urea oxidation reaction
2D/3D architecture

ABSTRACT

In this work, we fabricated an efficient pre-catalyst based on (Ni, Co)S_2 solid solution with hierarchical architecture and high porosity to boost urea oxidation reaction and electrocatalytic oxidation of organic small molecules. The interaction between Ni and Co can optimize the electronic structure, resulting in the improved conductivity and accelerated charge transfer rate. The 2D/3D architecture can enrich more active species and endow the mass and electron transport to facilitate the surface oxidation and the following catalytic process. Post-structure and catalytic characterizations confirm the surface oxidation of (Ni, Co)S_2 during the stability test, and the *in-situ* formed Co(Ni) based (oxy)hydroxides exhibit superior catalytic activity and facilitated charge transfer ability. As a result, the optimal (Ni, Co)S_2 solid solution pre-catalyst displays facilitated catalytic behavior and good stability for multifunctional electrocatalytic oxidation, in which a high conversion of benzyl alcohol (97.50%), a good selectivity to benzoic acid (93.78%) and a satisfied faraday efficiency (91.86%) can be achieved.

With the increasing global energy demands and environmental pollution, water electrolysis, as a promising route for hydrogen generation, has drawn much attention in recent years due to high conversion efficiency and reaction selectivity, ease of operation as well as zero emission of pollutant. However, a considerable high overpotential is usually necessary to realize water electrolysis owing to the sluggish four-electron transfer mechanism of the anodic oxygen evolution reaction (OER) [1]. Fortunately, electrocatalysis of small molecules, such as urea and hydrazine hydrate, could overcome this drawback by replacing the OER to couple with cathodic hydrogen evolution reaction (HER), realizing hydrogen production and pollution treatment simultaneously [2]. Notably, the thermodynamic equilibrium potential can decrease from 1.23 V to 0.37 V *vs.* the reversible hydrogen electrode (RHE) by using urea oxidation reaction (UOR) [3]. Besides, electrocatalytic oxidation (ECO) of alcohols and aldehydes into the carbonyl materials, is also highly promising to replace the OER to facilitate hydrogen generation and achieve value-added products [4]. Moreover, hazardous oxidants or O_2 with high pressure which are usually applied in the traditional organic oxidation synthesis can be avoided [5]. However, in either UOR or ECO, highly active electrocatalysts are necessary because of the multi-electron transfer process.

Transition metal sulfides (TMSs) based catalysts, strictly speaking, the "pre-catalysts", have been proved that usually exhibit superior catalytic activity to metal oxides because of the *in-situ* formed metal (oxy)-hydroxides on the surface of TMSs during electrocatalytic oxidation due to the polarized conditions, especially in a strong oxidation environment [6]. However, their catalytic behavior still cannot meet the need of industrial applications in electrocatalysis owing to the unsatisfied ability to enrich the active species and the unfulfilled electron transfer rate. Among the strategies to enhance the catalytic activity, polymetallic synergy is highly effective yet challenging route to improve the charge transfer rate and facilitate reaction kinetics [7,8]. For instance, Ni can react with Fe ions to optimize the electronic structure of Fe-based catalysts, resulting in the enhanced electrical conductivity and electron transport ability [9]. Moreover, the partial charge-transfer be-

* Corresponding authors.
E-mail addresses: haopin@sdnu.edu.cn (P. Hao), jiantian@sdust.edu.cn (J. Tian).
[1] These authors contributed equally to this work.

https://doi.org/10.1016/j.cclet.2022.107843
1001-8417/

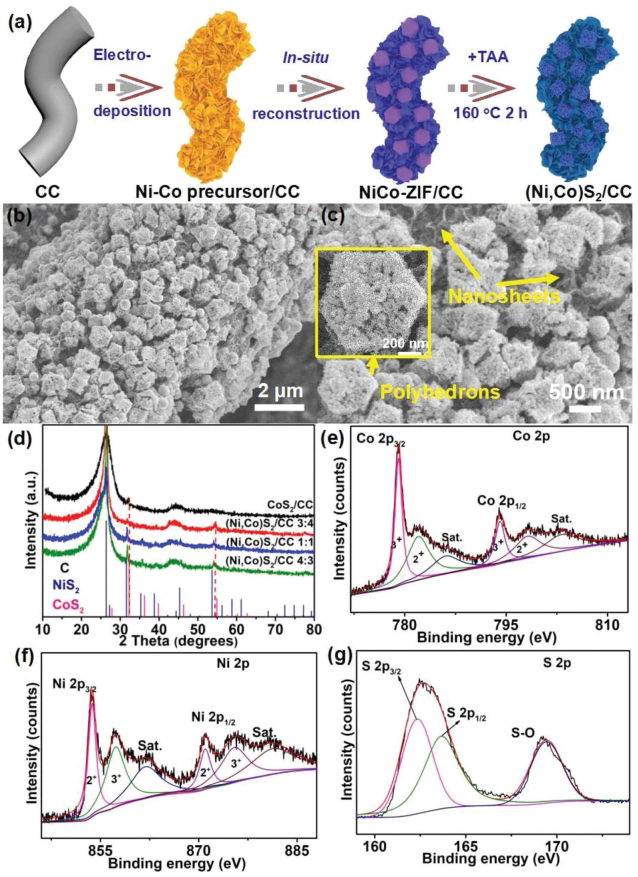

Fig. 1. (a) Schematic diagram of synthetic route. (b, c) SEM images of (Ni, Co)S_2/CC 1:1. (d) XRD patterns of catalysts. High-solution XPS spectra of (e) Co, (f) Ni, (g) S.

tween Ni and Fe can induce the generation of Ni^{3+} ions which are deemed as the active sites for electrocatalytic oxidation [10]. Besides, in order to enrich active species, construction of a hierarchical porous architecture with both 2D and 3D structures can not only shorten the diffusion channels to facilitate the mass and electron transport and enable more active species participating in the reaction, but also supply enough buffer spaces for stress release to ensure structure stability during continuous operation, further contributing to the robust catalytic activity, the rapid reaction kinetics as well as the excellent electrochemical stability [11,12]. In view of these premises, we deduced that constructing TMSs precatalysts with both 2D and 3D structures based on polymetallic synergy would be an effective strategy to enrich surface sites and facilitate electron transport, contributing to the promoted surface oxidation to boost the catalytic activity.

In this work, a multi-functional pre-electrocatalyst based on (Ni, Co)S_2 solid solution with 2D/3D porous polyhedron-on-sheet hierarchical structure was fabricated, and the synthetic route is shown in Fig. 1a. Firstly, the Ni-Co precursor with 2D nanosheet structure aligns on carbon cloths (CC) evenly *via* the electro-deposition method (Figs. S1a–d in Supporting information). Subsequently, the nanosheets, as the template to realize the structure reconstruction, coordinate with 2-methylimidazole (2-MeIM) to achieve the hierarchical architecture with both 2D and 3D characteristics. Scanning electron microscopy (SEM) images give strong evidence for the *in-situ* structural remodeling (Figs. S2a and b in Supporting information). New rhombic dodecahedrons are formed and grafted uniformly on the nanosheet layers after coordination, indicating the successful structure reformation. Transmission electron microscopy (TEM) image further identifies the solid characteristics and the intimately bound between dodecahedrons and nanosheets (Fig. S2c in Supporting information). The X-ray diffraction (XRD) pattern in Fig. S2d (Supporting information) identifies that all peaks can be indexed to the phase of ZIF-67 (NiCo-ZIF/CC). For sulfur addition, the NiCo-ZIF/CC precursors are hydrothermally vulcanized at 160 °C for 2 h. Figs. 1b and c show that the products keep the original structure of NiCo-ZIF/CC. However, the surface of polyhedrons appears coarse and porous, and the interior becomes hollow. Fig. S3 (Supporting information) further confirms a higher specific surface area (31.57 m^2/g) of the precursor after sulfuration than NiCo-ZIF/CC (10.10 m^2/g), which is attributed by the mesoporous structure of polyhedrons. As mentioned above, such porous hierarchical structure can ensure sufficient diffusion pathways for ion and mass transfer, and enrich more active species during oxidation process, resulting in the robust catalytic activity and facile reaction kinetics. Other splits with different levels of Ni incorporation display similar morphology in Fig. S4 (Supporting information).

XRD patterns in Fig. 1d reveal that the pristine sample without Ni incorporation after sulfurization is pure CoS_2 (JCPDS card No. 41–1471) except for the diffraction peaks of carbon (JCPDS card No. 41–1487), while the nearly identical peaks can be observed after Ni addition except for the weak shift from the (200) plane at 32.30° in CoS_2 towards the (200) plane at 31.59° in NiS_2 (JCPDS card No. 11–0099), indicating the formation of (Ni, Co)S_2 solid solution. Besides, as shown in the peak at 54.94°, the more the addition of nickel, the more obvious the shift to the plane of NiS_2 (53.65°). Valence state of the pre-catalyst ((Ni, Co)S_2/CC 1:1) was investigated by X-ray photoelectron spectroscopy (XPS). From Fig. 1e, we can see two dominated peaks can be divided into the spin-orbit doublets of Co $2p_{3/2}$ and Co $2p_{1/2}$, respectively. The energies at 782.0 and 798.2 eV are designated as Co^{2+} and the peaks at around 779.1 and 794.1 eV are assigned to Co^{3+} which is active for electro-oxidation [13,14]. Besides, two broad peaks located at 786.0 and 803.2 eV are the shakeup satellites. It should be noted that the characteristic peaks of Co^{3+} in (Ni, Co)S_2/CC 1:1 display a negative shift about 0.38 eV compared with CoS_2/CC, ascribing to the partial charge transfer between Ni and Co ions (Fig. S5a in Supporting information). For the high resolution profiles of Ni, the characteristic peaks of Ni^{2+} locate at 853.7 and 871.0 eV, while the peaks of Ni^{3+} anchor at 857.3 and 875.4 eV, confirming the successful incorporation of Ni for the generation of (Ni, Co)S_2 solid solution (Fig. 1f) [12,15]. Besides, two wide peaks at 861.8 and 881.2 eV represent the satellites. We can see that the peak intensity of Ni^{3+} increases obviously in (Ni, Co)S_2/CC, indicating the partial charge transfer between Ni and Co after Ni incorporation (Fig. S5b in Supporting information). In the sample of NiS_2/CC, the total peak area ratio of Ni^{3+} to Ni^{2+} is 0.94:1. However, this ratio in the sample of (Ni, Co)S_2/CC increases to 1.57:1, illustrating that a part of Ni^{2+} converted to Ni^{3+} due to the electron transfer from Ni to Co. Additionally, three peaks can be fitted in the high-resolution of S 2p, ascribing to the M-S bond, such as Ni-S and Co-S, at 162.3 and 163.6 eV, and S-O bond resulted by surface oxidation at 169.4 eV (Fig. 1g) [9].

TEM was employed to further identify the detailed structure of (Ni, Co)S_2/CC 1:1. Figs. 2a and b display the structure of thin nanosheet as well as the polyhedron with porous and hollow inherent features, confirming the 2D/3D porous multistage configuration. Fig. 2c displays the clear lattice which is about 0.24 nm, corresponding to the (210) facet of CoS_2 or NiS_2. The fast fourier transform (FFT) pattern originated from Fig. 2c verifies the single crystal essence of the solid solution. Element distribution was further probed *via* the energy dispersive spectrometry (EDS) analysis. As shown in Fig. 2d, Ni, Co and S disperse uniformly on the substrate, indicating the homogeneous composition of (Ni, Co)S_2 without partial element aggregation. The actual molar ratio of Ni to Co was identified as 1:0.99 by inductively coupled plasma op-

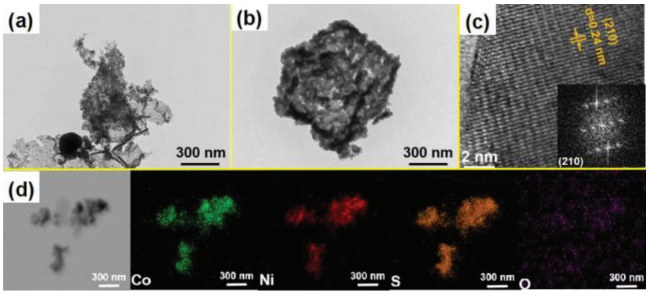

Fig. 2. Detailed structure of (Ni, Co)S_2/CC 1:1. (a, b) TEM, (c) HRTEM and the corresponding FFT image, (d) the element mapping.

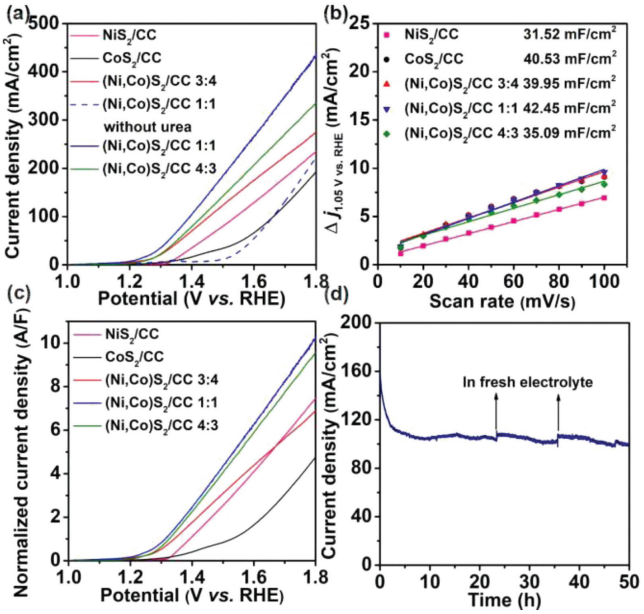

Fig. 3. (a) LSV curves for UOR without IR correction at 2 mV/s, (b) current density variation at 1.05 V *vs.* RHE as a function of scan rates, (c) LSV curves normalized by C_{dl}, (d) CA tests at 1.53 V for 50 h.

tical emission spectrometry (ICP-OES, Table S1 in Supporting information). The value is nearly the same with the addition ratio, confirming the successful incorporation of Ni in CoS_2.

It has been well accepted that the active metal species with high valence can be *in-situ* generated due to the surface oxidation of the pre-catalysts and thus facilitate the electrocatalytic oxidation behavior to realize urea splitting. Therefore, the UOR performance of as-prepared samples was evaluated through linear sweep voltammetry (LSV) measurement using a three-electrode setup in the electrolyte of 1 mol/L KOH with 0.33 mol/L urea. NiS_2 was fabricated in advance for performance comparison (Fig. S6 in Supporting information). As revealed in Fig. 3a, (Ni, Co)S_2/CC samples display a much lower onset potential than NiS_2/CC and CoS_2/CC, indicating the positive effect of Ni addition on the enhancement of UOR performance. For reaching a 10 mA/cm^2 current density, the lowest potential is presented by (Ni, Co)S_2/CC 1:1 (1.22 V *vs.* RHE), which is about 40–140 mV lower than other splits (Table S2 in Supporting information), confirming that the optimal molar ratio of Ni and Co is 1:1 to achieve the highest UOR activity. Of note, this significantly improved value is also the most attractive one among a series of advanced catalysts reported previously (Table S3 in Supporting information) [16–22]. To explore the intrinsic activity, electrochemical double-layer capacitance (C_{dl}), as a general factor to evaluate the electrochemical surface area (ECSA), was calculated to diminish the morphology benefits of porous multistage structure (Fig. 3b and Fig. S7 in Supporting information) [12]. The structure reconstruction with 2D/3D porous configuration results in a much higher C_{dl} value of 42.45 mF/cm^2, demonstrating the important role of the 2D nanosheet morphology grafting with 3D porous polyhedrons of the (Ni, Co)S_2/CC pre-catalysts on fertilizing the reactive surface sites for the surface oxidation process to *in-situ* generated active species. Fig. 3c is the corresponding LSV profiles normalized by C_{dl}. As expected, the (Ni, Co)S_2/CC 1:1 exhibits the superior intrinsic activity to its counterparts, further confirming the synergistic effects of nickel and cobalt on the enhancement of catalytic activity. Besides, Tafel plots in Fig. S8a further confirm the facile UOR kinetics of the catalysts. (Ni, Co)S_2/CC 1:1 reveals the smallest Tafel slope about 109 mV/dec, which is much smaller than NiS_2 (138 mV/dec) and CoS_2 (183 mV/dec), possibly ascribing to the facilitated mass and charge pathways, the boosted electron transfer rate as well as the enhanced conductivity. Electrochemical impedance spectra (EIS) were measured at 1.40 V *vs.* RHE to further identify the above reasons (Fig. S8b and Table S2). Improved electrical conductivity and electron transport ability can be observed after Ni incorporation, revealing that the interaction between Ni and Co can optimize the electronic structure of CoS_2, contributing to the favorable charge transport behavior of (Ni, Co)S_2/CC samples for the combined surface oxidation and UOR process. Among them, (Ni, Co)S_2/CC 1:1 shows the smallest charge transfer resistance (R_{ct}) of 2.13 Ω.

In addition, the chronoamperometry (CA) test was conducted at 1.53 V and 1.35 V to further identify the surface oxidation and assess the long-term durability of the (Ni, Co)S_2/CC 1:1 pre-catalyst (Fig. 3d and Fig. S9 in Supporting information). We can see that a sharp decrease was happened in the first 2 h, which may be ascribed to the delayed removal of CO_3^{2-} ions, thus leading to the rapid reduction of the surface active sites for the subsequent UOR. Fortunately, as the catalytic process proceeds, steady catalytic behavior can be confirmed, resulting in high current retention rates of 93.40% and 94.90% after 50 h continuous UOR at 1.53 V and 1.35 V, respectively. This can be ascribed to the surface oxidation process without structural transformation and the high porosity as the stress buffer basin. Therefore, the morphological change of the catalyst can be ignored after constant redox reaction (Fig. S10 in Supporting information). In order to identify the relationship between the catalytic activity and the *in-situ* formed surface active species, the LSV curves before and after the CA tests at different times were recorded. From Fig. S11a (Supporting information), we can see the LSV curves after 1 h are obviously different from the initial one, indicating the surface phase of the pre-catalyst has been changed, which can be proved by the XPS results. As depicted in Fig. S12 (Supporting information), the peak intensity of O 1s increases markedly, while the intensity of S 2p peak dramatically decreases along with the increase of the test time. Meanwhile, the gradual increment of the current density can be observed, revealing that the surface oxidation of the pre-catalyst is actually a process for activation. Besides, EIS data display the reduced R_{ct} value after the first two hours of testing, illustrating the accelerated reaction kinetics for the surface oxidation and UOR (Fig. S11b in Supporting information). Until 50 h, XPS spectra show that the peaks of S 2p nearly disappear accompanying with the significantly enhanced peak of O 1s, indicating the completely surface oxidation of (Ni, Co)S_2 to the metal (oxy)hydroxides (Figs. S13a and b in Supporting information). Meanwhile, the proportion of active Ni^{3+} significantly surpasses the Ni^{2+} in the high resolution profiles of Ni after 50 h. CA test, further confirming the important effect of the surface oxidation to boost active sites for promoted electrocatalytic oxidation (Figs. S13c and d in Supporting information). Generally, these *in-situ* generated species cannot be identified by XRD due to the amorphous nature or too thin layer on the surface of the pre-catalyst. However, the dense hot spots of O in the re-

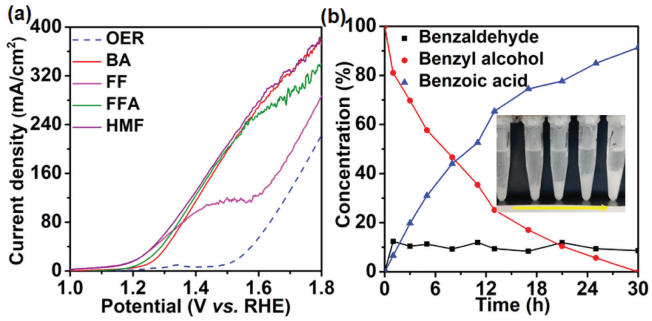

Fig. 4. (a) LSV curves for ECO, (b) conversion and selectivity for ECO in 1.0 mol/L KOH with 100 mmol/L BA at 1.43 V for 30 h. The inset is the photo of products during ECO.

sults of EDS mapping after CA test can also confirm the surface transformation from (Ni, Co)S_2/CC into the corresponding metal (oxy)hydroxides accompanied by S loss during the UOR to form the unique (Ni, Co)S_2@Co(Ni) based (oxy)hydroxides core-shell structure on CC (Fig. S13e in Supporting information).

For the purpose to investigate the multi-functional catalytic activity of (Ni, Co)S_2/CC 1:1, the LSV curves in 1 mol/L KOH with different organic molecules, involving benzyl alcohol (BA), 5-hydroxymethylfurfural (HMF), furfuryl alcohol (FFA) and furfural (FF), are drawn in Fig. 4a. The catalyst demonstrates a much higher activity on ECO of these organic molecules than water, implying a high preference to electro-oxidize organic species. Fig. 4b displays the conversion and selectivity for ECO in 1.0 mol/L KOH with 100 mmol/L BA at 1.43 V *vs.* RHE for 30 h. The concentration of benzoic acid increases linearly with ECO time, while the amount of BA is getting less and less. Finally, a high conversion of BA about 97.50% and an excellent selectivity to benzoic acid about 93.78% can be achieved. The Faraday efficiency (FE) has been calculated to be as high as 91.86%. The inset in Fig. 4b is the photo of products during 30 h ECO operation. We can see that as the reaction time lengthens, the white powder becomes moreand more, confirming the mass production of benzoic acid.

In conclusion, a novel multi-functional pre-electrocatalyst based on (Ni, Co)S_2 solid solution with well-designed hierarchical structure and high porosity was fabricated. The interaction between Ni and Co can optimize the electronic structure, resulting in the improved conductivity and accelerated charge transfer rate. In addition, the 2D/3D architecture can enrich more active species and endow the mass and electron transport to facilitate the surface oxidation and the following electrocatalytic oxidation process. Post-structure and catalytic characterizations confirm the surface oxidation of (Ni, Co)S_2/CC during the stability test, and the *in-situ* formed Co(Ni) based (oxy)hydroxides exhibit superior catalytic activity and facilitated charge transfer ability, contributing to the impressive multifunctional performance and making the NiCo-based sulfide solid solution as a promising pre-catalyst for hydrogen production with the treatment of nitrogenous wastewater and the acquisition of value-added products synchronously.

Declaration of competing interest

The authors declare that they have no known competing financial interests or personal relationships that could have appeared to influence the work reported in this paper.

Acknowledgments

This work was supported by National Natural Science Foundation of China (Nos. 21927811, 51602182, 21808129) and the Natural Science Foundation of Shandong Province, China (No. ZR2021ME032).

Supplementary materials

Supplementary material associated with this article can be found, in the online version, at doi:10.1016/j.cclet.2022.107843.

References

[1] X. Wang, L. Yu, B.Y. Guan, S. Song, X.W. Lou, Adv. Mater. 30 (2018) 1801211.
[2] L. Wang, Y. Zhu, Y. Wen, et al., Angew. Chem. Int. Ed. 60 (2021) 10577–10582.
[3] P. Hao, W. Zhu, L. Li, et al., Electrochim. Acta 338 (2020) 135883.
[4] Z. Li, J. Zhang, X. Jing, et al., J. Mater. Chem. A 9 (2021) 6152–6159.
[5] X. Chen, X. Zhong, B. Yuan, et al., Green Chem. 21 (2019) 578–588.
[6] M. Zhou, Q. Weng, X. Zhang, et al., J. Mater. Chem. A 5 (2017) 4335–4342.
[7] A. Haeussler, S. Abanades, J. Jouannaux, et al., AIMS Mater. Sci. 6 (2019) 657–684.
[8] Z. Ji, Y. Song, S. Zhao, et al., ACS Catal. 12 (2022) 569–579.
[9] P. Hao, Y. Xin, J. Tian, et al., Sci. Chin. Chem. 63 (2020) 1030–1039.
[10] P. Hao, W. Zhu, L. Li, et al., Chem. Commun. 55 (2019) 10138–10141.
[11] K. Rui, G. Zhao, Y. Chen, et al., Adv. Funct. Mater. 28 (2018) 1801554.
[12] P. Hao, H. Wen, Q. Wang, et al., J. Mater. Chem. A 9 (2021) 8576–8585.
[13] H. Tan, Z. Liu, D. Chao, et al., Adv. Energy Mater. 8 (2018) 1800685.
[14] Y. Lu, D. Fan, Z. Chen, et al., Sci. Bull. 65 (2020) 460–466.
[15] F. Li, P. Wang, X. Huang, et al., Angew. Chem. Int. Ed. 58 (2019) 7051–7056.
[16] Q. Zhang, F.M. Kazim, S. Ma, et al., Appl. Catal. B 280 (2021) 119436.
[17] Z. Cao, T. Zhou, X. Ma, et al., ACS Sustain. Chem. Eng. 8 (2020) 11007–11015.
[18] H. Liu, S. Zhu, Z. Cui, et al., Nanoscale 13 (2021) 1759–1769.
[19] Q. Li, N. Li, J. An, H. Pang, Inorg. Chem. Front. 7 (2020) 2089–2096.
[20] W. Han, X. Li, L. Lu, et al., Chem. Commun. 56 (2020) 11038–11041.
[21] M. Yuan, X. Guo, N. Li, H. Pang, J. Colloid Interface Sci. 589 (2021) 56–64.
[22] N. Chen, Y. Du, G. Zhang, W. Lu, F. Cao, Nano Energy 81 (2021) 105605.